Nanoscaled La$_{0.6}$Sr$_{0.4}$CoO$_{3-\delta}$ as intermediate temperature solid oxide fuel cell cathode: Microstructure and electrochemical performance

Jan Hayd [a,b,*], Levin Dieterle [b,c], Uwe Guntow [d], Dagmar Gerthsen [b,c], Ellen Ivers-Tiffée [a,b]

[a] Institut für Werkstoffe der Elektrotechnik (IWE), Karlsruher Institut für Technologie (KIT), Adenauerring 20b, 76131 Karlsruhe, Germany
[b] DFG Center for Functional Nanostructures (CFN), Karlsruhe Institute of Technology (KIT), 76131 Karlsruhe, Germany
[c] Laboratorium für Elektronenmikroskopie (LEM), Karlsruher Institut für Technologie (KIT), 76131 Karlsruhe, Germany
[d] Fraunhofer-Institut für Silikatforschung (ISC), 97082 Würzburg, Germany

ARTICLE INFO

ABSTRACT

Lowering the operation temperature of solid oxide fuel cells to the range of 400–600 °C has generated new concepts for materials choice, interfacial design and electrode microstructures. In this study nanometer scaled and nanoporous La$_{0.6}$Sr$_{0.4}$CoO$_{3-\delta}$ (LSC) was derived from metal-organic precursors as thin film cathodes of about 200 nm thickness with mean grain sizes ranging from 17 to 90 nm and porosities of up to 45%. These microstructures resulted from different processing parameters such as heating rate, calcination temperature and post calcination annealing, and made it possible to study the influence of the electrode microstructure on the electrochemical performance. Microstructural characteristics were analyzed by scanning and transmission electron microscopy and the performance was evaluated in terms of area specific polarization resistance by means of electrochemical impedance spectroscopy in a temperature range of 400–600 °C. Polarization resistances as low as 0.023 Ω cm^2 were measured at 600 °C, facilitated by a substantial increase of the inner surface area of the nanoscaled microstructure, resulting from low temperature processing at ≤800 °C, and by enhanced catalytic properties determined for nanoscaled La$_{0.6}$Sr$_{0.4}$CoO$_{3-\delta}$ prepared by metal organic deposition.

© 2010 Elsevier B.V. All rights reserved.

1. Introduction

A major target of solid oxide fuel cell (SOFC) research is the reduction of the operating temperature from currently 700–1000 °C to an intermediate temperature range of 500–700 °C or lower. Especially for the application of SOFCs in auxiliary power units (APUs) [1] or μ-SOFCs [2] low operation temperatures are a key factor. Degradation is expected to be reduced at lower temperatures and material costs for insulation, housing and interconnects are expected to be reduced as well, since a greater variety of suitable materials and especially considerably less expensive materials are available [3]. However, as the durability requirements for these inactive parts of a SOFC system decrease with temperature, the losses of the electrochemically active electrodes and the electrolyte heavily increase and must be compensated by a combination of material and geometry related improvements. In the case of a cathode, the increasing polarization losses with decreasing operating temperature can be counteracted by the application of a highly electrochemically active material and an optimized microstructure. The latter however depends on the targeted operation temperature and material related properties [4–6].

A promising candidate for intermediate temperature application is strontium substituted lanthanum cobalt oxide (La,Sr)CoO$_{3-\delta}$, a perovskite-type material with a mixed ionic and electronic conductivity (MIEC) at elevated temperatures [7–9]. Compared to the state of the art material (La,Sr)(Co,Fe)O$_{3-\delta}$, it exhibits better catalytic properties [10]. In addition, a pronounced degradation caused by carbonate formation resulting from the CO$_2$ contained in ambient air – as it is the case for other candidates for intermediate temperature operation such as (Ba,Sr)(Co,Fe)O$_{3-\delta}$ [11] – has so far not been reported about.

In a recent publication [6], impressive performance data have already been presented, demonstrating the potential of metal organic deposition (MOD) derived nanoscale cathodes and outlining the improvement that has been achieved since the first profound investigations by Peters et al. [8]. In the following, a systematic variation of the microstructure, resulting from processing variations, is presented and the influence of the microstructure in terms of grain size and porosity on the cathode performance is assessed in the temperature range of 400 °C < T < 600 °C by means of electrochemical impedance spectroscopy. Furthermore, the measured data is compared with literature data.

* Corresponding author at: Institut für Werkstoffe der Elektrotechnik (IWE), Karlsruher Institut für Technologie (KIT), Adenauerring 20b, 76131 Karlsruhe, Germany. Tel.: +49 721 6087573; fax: +49 721 6087492.
E-mail address: jan.hayd@kit.edu (J. Hayd).

Table 1
Processing parameters of the high temperature step for sample preparation.

Parameter	Value	Explanation
T_{max}	700 °C, 800 °C	Maximum processing temperature
ΔT	3 K min^{-1}, >200 K min^{-1} (RTA)	Heating rate
t_{an}	0 h, 10 h, 100 h	Annealing time at T_{max}

2. Experimental

2.1. Sample preparation

The nanoscaled cathodes were applied as thin films by a wet chemical route called metal organic deposition. In this sol–gel based method propionates of La, Sr and Co were prepared as solid precursors separately, which were then dissolved in propionic acid at room temperature in the aimed stoichiometry $La_{0.6}Sr_{0.4}CoO_{3-\delta}$ (LSC). The precursors were derived from $La_2(CO_3)_3$, $Co(OH)_2$ and Sr metal by the reaction with propionic acid (in excess) in the presence of propionic acid anhydride. Best results in terms of homogeneous and crack free thin films were obtained with a solution containing 10 mass% of the resulting oxide which exhibited a kinematic viscosity of 3.67×10^{-6} m^2 s^{-1} at 20 °C. Inductively coupled plasma-atomic emission spectroscopy (ICP-AES) was used to measure the final composition of the coating sol.

The thin film cathodes were applied onto thin (400–800 μm, $d \approx 25$ mm) $Ce_{0.9}Gd_{0.1}O_{1.95}$ (GCO) electrolyte pellets (Daiichi Kigenso Kagaku Kogyo Co. Ltd., Japan) by a single dip coating step with a withdraw rate of 8 cm min^{-1}. In a subsequent drying process at room temperature for 5 min, followed by a rapid thermal annealing (RTA) step at 170 °C for 5 min, all volatile components were removed from the coating. In a second high temperature step, the actual perovskite phase was formed. In this step, different heating rates, rapid thermal annealing or a slow heating with a heating ramp of $\Delta T = 3$ K min^{-1}, different maximum processing temperatures of $T_{max} = 700$ °C or 800 °C, and different annealing times of $t_{an} = 0$ h, 10 h and 100 h were applied, resulting in different microstructures of the thin film cathodes. In the case of an annealing time of $t_{an} = 0$ h, the sample was only heated up to T_{max} and was then immediately cooled down to room temperature, without any further annealing at T_{max}. The different high temperature processing parameters are summarized in Table 1.

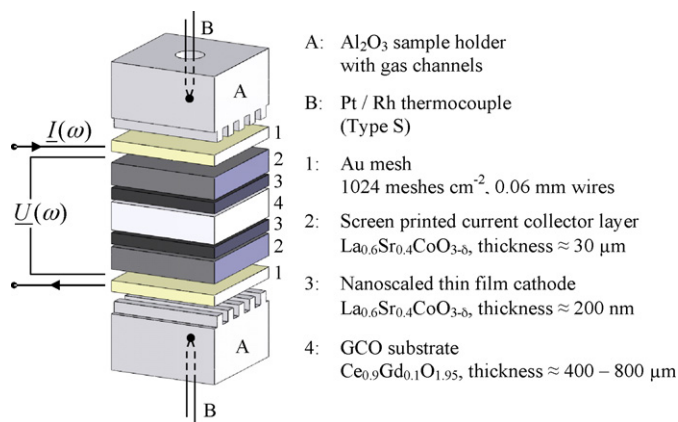### 2.2. Microstructural and chemical analysis

The resulting microstructures were analyzed by scanning electron microscopy (SEM) (Zeiss 1540XB, Carl Zeiss NTS GmbH). Grain sizes were determined from surface SEM micrographs using the image processing software SPIP^{TM} (Image Metrology A/S). The

Table 2
Microstructural properties of nanoscaled thin film cathodes prepared with $\Delta T = 3$ K min^{-1}. $d_{mean,TEM}$ denotes the mean grain size determined by TEM analysis, $d_{mean,SEM}$ the mean grain size determined by SEM analysis. ε denotes the porosity determined by STEM tomography.

Processing of sample		$d_{mean,TEM}$ (nm)	$d_{mean,SEM}$ (nm)	ε (vol.%)
T_{max} (°C)	t_{an} (h)			
700	0	17 ± 5	16.4 ± 7.82	45 ± 10
700	10	ND	25.0 ± 11.4	ND
700	100	28 ± 10	30.2 ± 14.1	ND
800	0	29 ± 10	27.0 ± 10.6	17 ± 5
800	10	ND	38.8 ± 18.8	ND
800	100	90 ± 33	63.5 ± 33.5	ND

ND, not determined.

A: Al$_2$O$_3$ sample holder with gas channels

B: Pt / Rh thermocouple (Type S)

1: Au mesh 1024 meshes cm^{-2}, 0.06 mm wires

2: Screen printed current collector layer La$_{0.6}$Sr$_{0.4}$CoO$_{3-\delta}$, thickness ≈ 30 μm

3: Nanoscaled thin film cathode La$_{0.6}$Sr$_{0.4}$CoO$_{3-\delta}$, thickness ≈ 200 nm

4: GCO substrate Ce$_{0.9}$Gd$_{0.1}$O$_{1.95}$, thickness ≈ 400 – 800 μm

Fig. 1. Schematic of the measuring setup for EIS analysis of a symmetrical cell consisting of a μm sized LSC current collector, a LSC thin film cathode and a GCO electrolyte substrate.

mean grain-size $d_{mean,SEM}$ was calculated as a circle equivalent diameter from the grain area, averaging over at least 288 grains. A more detailed microstructural characterization was done by transmission electron microscopy (TEM) with a 200 keV Philips CM200 FEG/ST equipped with a field emission gun. Furthermore, high-angle annular dark-field (HAADF) scanning TEM (STEM) tomography performed on a FEI Titan3 80-300 was used for the determination of porosity values. TEM plan view samples were prepared by dimpling and Ar-ion milling. Cross-section samples were prepared by single-sector ion milling at 4° and an ion energy of 3–4 keV resulting in a nearly plan-parallel sample profile [12]. Again, grain-sizes ($d_{mean,TEM}$) were determined as described before. For each sample between 120 and 150 grains were analyzed using the image processing software ImageJ (http://rsbweb.nih.gov/ij/). However, only grains which exhibited a good contrast to the surrounding grains in the TEM bright-field images (plan-view) were evaluated. The porosity ε was determined by means of a 3D tomography reconstruction of the thin film cathodes using the simultaneous iterative reconstruction technique (SIRT) [13]. This was done for two samples only, as it is rather complex and time consuming. X-ray diffraction (XRD) (Siemens D5000, Bruker-AXS) was used to investigate crystallization and chemical homogeneity. The setup was operated in the grazing incidence mode with a tube angle of 1.5° using a copper radiation source (CuKα_1, $\lambda = 0.15406$ nm) and a monochromator (Bruker-AXS) on the detector side.

2.3. Electrochemical characterization

Electrochemical characterization was performed by means of impedance spectroscopy on a symmetrical cell setup as outlined in Fig. 1. The nanoscaled thin film cathodes with an active cell area of 1 cm × 1 cm were contacted by a uniform, screen printed current collector layer (CCL) of μm sized La$_{0.6}$Sr$_{0.4}$CoO$_{3-\delta}$ of the same dimensions, which was dried for 12 h at 60 °C. The lateral conductivity of the thin film cathode itself is by far not sufficient to be contacted with a gold mesh only. The current collector layer was then contacted by a gold mesh (>99.99% Au, 1024 meshes cm^{-2}, 0.06 mm wires) leading to a homogeneous current distribution over the electrode and a low contact resistance [14]. This setup was then sandwiched between two Al$_2$O$_3$ blocks with gas channels and a weight of 150 g was applied on top of the setup. The LSC for the current collector layer was synthesized by a mixed oxide route (calcination at 1050 °C for 10 h), grinded down on a rolling bench to a mean particle size of $D_{50} = 1.8$ μm, and mixed with an organic binder (60 mass% solids content), resulting in the screen

printing paste. As high sintering temperatures would destroy the nanoscaled thin film cathode, the current collector layer was used in an unsintered state and the organics of the screen printing paste were burned out during the heating phase of the cell test. Electrochemical impedance spectroscopy (EIS) measurements were carried out in stagnant ambient air in temperature steps of 25 K from 400 to 600 °C using a Solartron 1260 frequency response analyzer in a frequency range of $10^{-1} < f < 10^{6}$ Hz. The amplitude of the current stimulus was chosen in order to achieve a voltage response of less than 50 mV. All experiments within this study were conducted under open circuit conditions (OCC). The impedance data were then analyzed by calculating and analyzing the corresponding distribution function of relaxation times (DRTs) [15] and CNLS fitting with the software package Z-View® (v2.8, Scribner Associates Inc.).

3. Results and discussion

3.1. Microstructure and XRD analysis

All samples prepared by MOD applying a slow heating rate of 3 K min^{-1} led to crack-free thin films with a nanoscaled microstructure as shown in Fig. 2(a). However, if the samples were processed with rapid thermal annealing, they exhibited a very inhomogeneous structure with bulges and cracks (Fig. 2(b)). In the following, the focus will lay on the slowly heated samples, as they exhibited a homogeneous microstructure. The RTA prepared samples were included to give an overview of the microstructures which can be derived by MOD technique.

Fig. 3 depicts high resolution SEM micrographs of the different surface morphologies of nanoscaled cathodes processed with a slow heating rate of 3 K min^{-1}. Controlled by the maximum processing temperature and annealing time, cathodes with mean grain sizes ranging from 17 nm to 90 nm and porosities of up to 45% were obtained. Both the smallest mean grain size and the highest porosity were determined for the sample calcined at 700 °C without further annealing (Fig. 3(a)). A detailed compilation of the microstructural data can be found in Table 2.

The mean grain sizes determined with the two methods are in good agreement. Only for large grain sizes, the results differ significantly. This is most likely a result of overlapping grains that partly cover each other – if observed from the surface – leading to an underestimation of the grain size by SEM surface analysis. In the following, particle sizes determined by TEM will be used. For those samples, where no TEM data is available, SEM derived data will be applied. As expected, the grain size increases with increasing maximum processing temperature and with increasing annealing time. The porosity decreases with increasing maximum processing temperature and with increasing annealing time. One coating step resulted in an average layer thickness of approximately 200 nm. An additional publication including more details and results of the microstructural and chemical investigations performed on these samples is currently in preparation.

The cross-sectional images Fig. 4(a) and (b) give a visual impression of the large range of grain sizes which can be obtained by MOD. The two images represent the upper and lower bound in terms of porosity and particle size. Fig. 4(c) and (d) depicts thin film cathode samples processed with the same parameters as the samples in (a) and (b), respectively, except for the heating rate. Representative for all samples prepared by rapid thermal annealing, these cathodes exhibited a dense surface layer with a high closed porosity underneath. We attribute this to a rapid heating of the coating's surface, which immediately formed a dense oxide surface layer. The gaseous decomposition products of the metal organics from the material underneath then lead to a high, closed porosity and large cavities beneath the dense surface layer. As grain sizes vary significantly over the cathode surface for these samples, no exact values could be determined. However, the RTA processed samples exhibited more or less the same grain growth behavior with temperature and temper time as the samples prepared applying the slow heating rate. For the porosity no clear trend was observed, as it was not possible to obtain reliable data. This was due to strong local variations of the porosity and a frequent occurrence of large cavities, which were still present in the sample annealed for 100 h at 800 °C.

X-ray diffraction analysis confirmed phase pure La$_{0.6}$Sr$_{0.4}$CoO$_{3-\delta}$ formation for the thin film cathodes [16,17]. An X-ray diffraction pattern of a nanoscaled thin film cathode processed at 700 °C ($\Delta T = 3$ K min^{-1}) and without further annealing is plotted in Fig. 5. This shows, that a temperature treatment at 700 °C is sufficient for the formation of phase pure LSC derived by MOD. The rather broad LSC related peaks result from the nanoscaled grain size. Secondary phases, e.g. reaction products between LSC and GCO, were not detected, which is in agreement with [18,19], as they are not expected to form.

3.2. EIS analysis

In Fig. 6, a Nyquist plot of a typical electrochemical impedance measurement is illustrated. The spectrum can be deconvoluted into the following contributions. R_0 is a combination of losses caused by the GCO electrolyte and ohmic losses within the electrodes and the current collector layer. It corresponds well to the ohmic losses associated with the electrolyte substrate. In this example, the theoretical value of the ohmic losses resulting from an on average 785 μm thick electrolyte at 600 °C is 3.83 ± 0.13 Ω cm^2. A conductivity of the electrolyte material of 2.05 ± 0.07 S m^{-1} at 600 °C was determined beforehand in a 4-probe DC conductivity experiment. ASR_{pol} sums up all cathodic losses. These include losses associated with the electrochemical reaction (ASR_{chem}) and the gas diffusion (ASR_{gas}). The latter results from gas diffusion limitations, which occur primarily in the stagnant gas within the gas channels of the Al$_2$O$_3$ contact block above the cathode surface and in the pores of the LSC current collector layer. They are predominant at low frequencies [8] and for temperatures of 500 °C and higher, they appear as a separate arc, as displayed in Fig. 6. However, these losses only
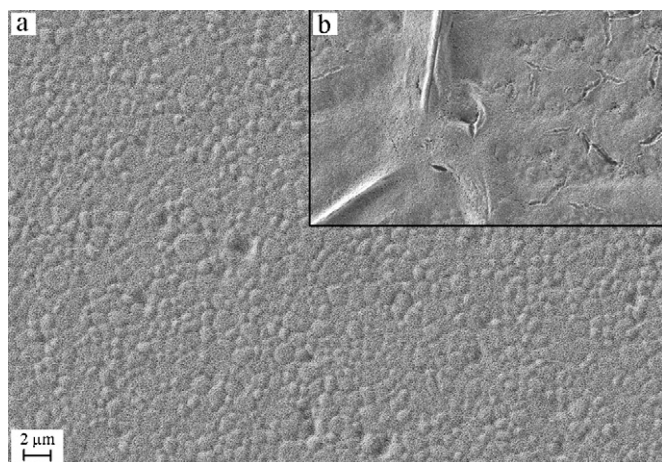
Fig. 2. Low magnification SEM micrographs of thin film cathodes on a GCO electrolyte substrate prepared with the processing parameters (a) $\Delta T = 3$ K min^{-1}, $T_{max} = 800$ °C, $t_{an} = 10$ h and (b) $\Delta T =$ rapid thermal annealing (RTA), $T_{max} = 800$ °C, $t_{an} = 10$ h. Thin film layers processed with a slow heating rate exhibited no cracks or areas of inhomogeneity over the whole substrate surface. The pattering of the layer is a result of the topography of the grains and grain boundaries of the electrolyte substrate. RTA led to a bulgy layer with cracks.
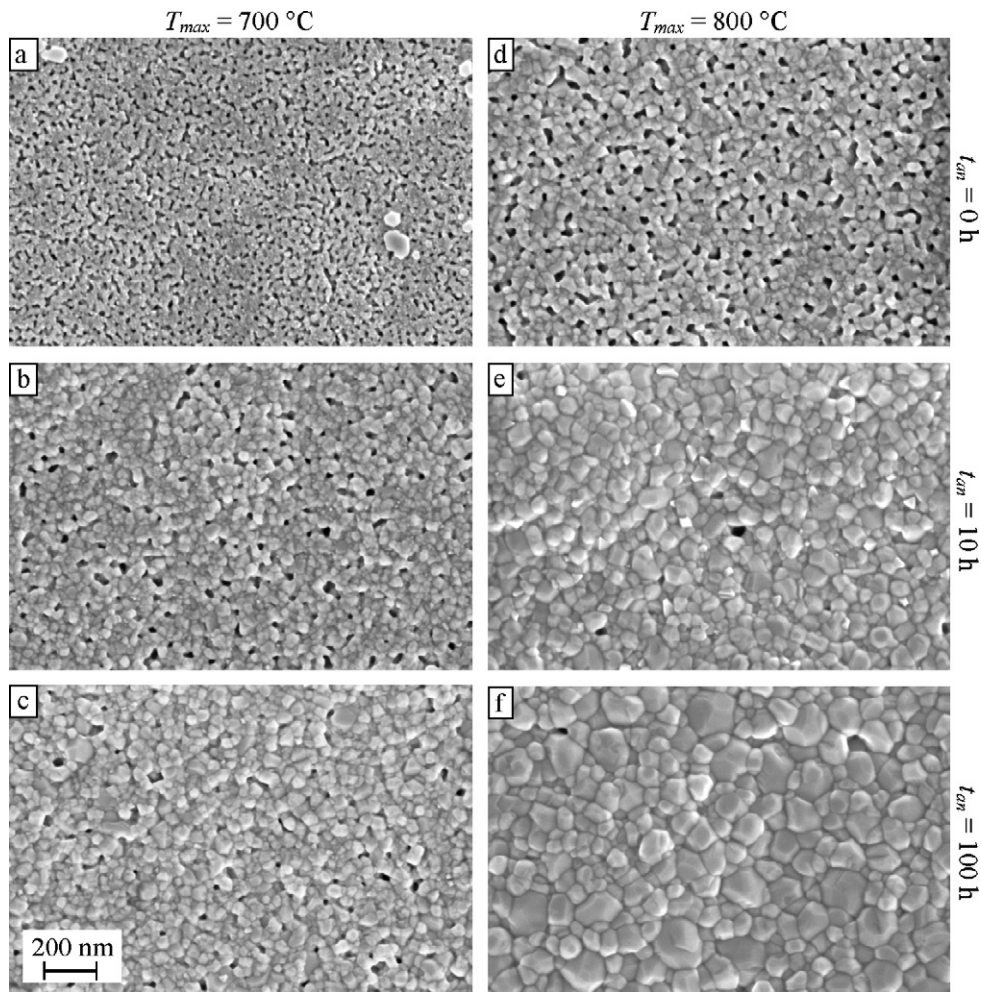
$T_{max} = 700\ ^{\circ}C$ $T_{max} = 800\ ^{\circ}C$

Fig. 3. SEM surfaces micrographs of nanoscaled cathodes processed at (a–c) 700 °C and (d–f) 800 °C for up to 100 h ($\Delta T = 3\ K\ min^{-1}$ for all samples).

occur in a testing setup with stagnant air as oxidant gas or at low oxygen partial pressures [7,20]. Under normal SOFC operating conditions with a steady oxidant gas gas-flow and a high oxygen partial pressure they can be neglected and will therefore be disregarded in the following.

3.3. Influence of the current collector on the cathode performance

To be really sure, that the measured ASR_{chem} is a contribution of the nanoscaled thin film only, not including any contributions of the current collector layer, this possible source of a systemat-
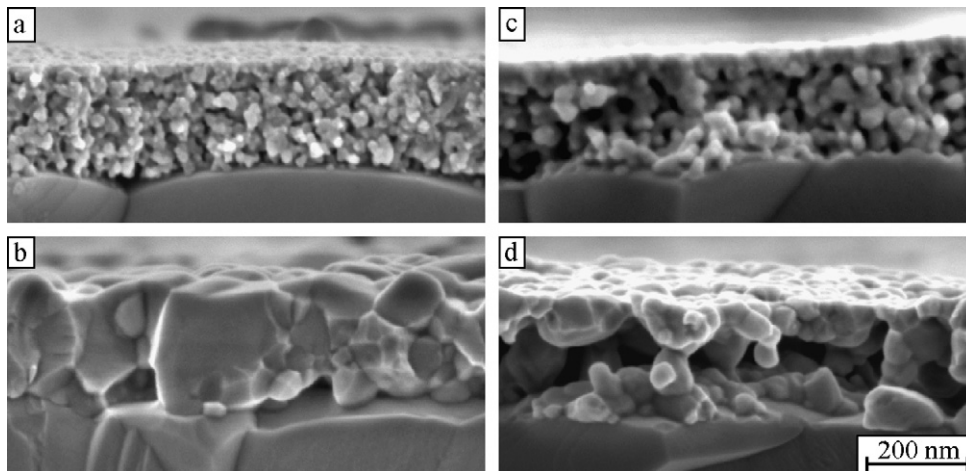

Fig. 4. SEM micrographs of nanoscaled cathode cross-sections of samples processed at (a) $\Delta T = 3\ K\ min^{-1}$, $T_{max} = 700\ ^{\circ}C$, $t_{an} = 0\ h$, (b) $\Delta T = 3\ K\ min^{-1}$, $T_{max} = 800\ ^{\circ}C$, $t_{an} = 100\ h$, (c) $\Delta T = RTA$, $T_{max} = 700\ ^{\circ}C$, $t_{an} = 0\ h$ and (d) $\Delta T = RTA$, $T_{max} = 800\ ^{\circ}C$, $t_{an} = 100\ h$.
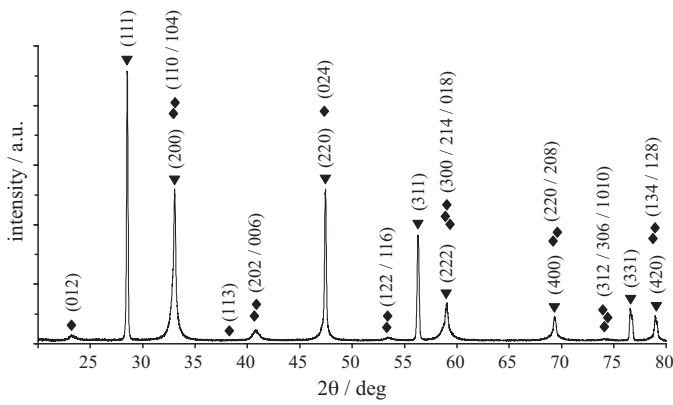
Fig. 5. XRD pattern of a MOD derived nanoscaled $La_{0.6}Sr_{0.4}CoO_{3-\delta}$ thin film cathode on a $Gd_{0.1}Ce_{0.9}O_{1.95}$ electrolyte processed with $\Delta T = 3\,K\,min^{-1}$, $T_{max} = 700\,°C$ and $t_{an} = 0\,h$; ♦ denotes the position of $La_{0.6}Sr_{0.4}CoO_{3-\delta}$ peaks [16] and ▼ those of $Ce_{0.9}Gd_{0.1}O_{1.95}$ [17].
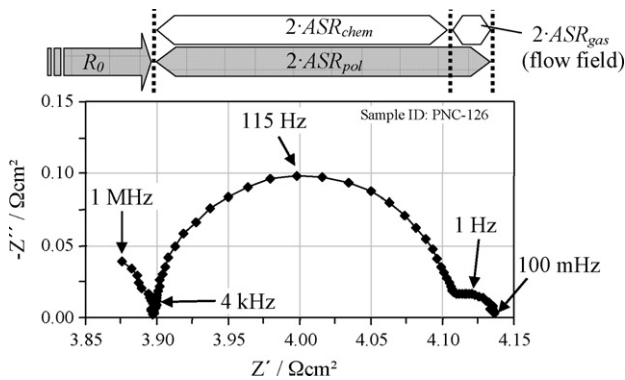
Fig. 6. Electrochemical impedance spectrum of a nanoscaled thin film cathode ($\Delta T = 3\,K\,min^{-1}$, $T_{max} = 800\,°C$, $t_{an} = 10\,h$) in form of a Nyquist plot, measured in a symmetrical setup at 600 °C in stagnant ambient air.

ical error must be considered carefully. As already mentioned in the experimental section, a gold mesh only would lead to high ohmic losses within the thin film cathode and therefore to areas of reduced activity. This is caused by a low lateral electronic conductivity in between the contact points of the gold mesh nods (distance ≈ 250 μm), resulting from the low film thickness. To improve this, pastes of μm sized particles of noble metals (silver, gold or platinum) or – as it is the case here – a paste of the same material as the thin film cathode is applied on top of the cathode to serve as a current collector. In some cases, the material selection is motivated by the materials properties. In [21] Au is preferred to Pt, to avoid possible influences of the catalytic properties of Pt on the electrochemical reaction. However, how large are these influences in reality? Determining the polarization losses of a cathode made of the current collector layer only will clarify this aspect. This can be done either theoretically by an appropriate model or experimentally. Starting with the calculation of the electrochemical characteristic of the current collector layer in terms of area specific polarization losses, a 1D model by Adler et al. [7] for a semi-infinite porous mixed conducting cathode with a fast

ionic transport, a high electronic conductivity and no gas phase limitations was applied. In a later publication Adler even applied the model on $(La,Sr)CoO_{3-\delta}$ type perovskite cathodes [19]. As the penetration depth of the electrochemical reaction δ (less than a few microns for a μm-scaled $La_{0.6}Sr_{0.4}CoO_{3-\delta}$ cathode [19]) is considerably smaller than the cathode thickens $l_{Cat} \approx 30\,μm$, the following expression can be used to calculate the polarization losses:

$$ASR_{chem} = \frac{R \cdot T}{4 \cdot F^2} \cdot \sqrt{\frac{\tau}{(1-\varepsilon) \cdot c_V \cdot D_V \cdot a \cdot r_O \cdot (\alpha_f + \alpha_b)}} \quad (1)$$

where c_V is the vacancy concentration within the MIEC material, D_V is the vacancy diffusion coefficient, r_O is the exchange neutral flux density and α_f and α_b are kinetic parameters of order unity. These parameters are material related and were taken from [19]. The geometry related parameters solid phase tortuosity τ and volume specific surface area a were calculated with the aid of a 3D finite element method (FEM) microstructure model by Rüger et al. [22] in combination with a correction term, determined by a focused ion beam (FIB) tomography 3D reconstruction of a real electrode structure [23]. The porosity ε is also a geometry related parameter and was determined by SEM analysis. F is the faraday constant, R the gas constant and T the absolute temperature.

The current collector layer used in this study exhibited an average particle size of 1.8 μm and a porosity of $\varepsilon = 0.4$ was estimated from SEM micrographs. The tortuosity and the volume specific surface area were then calculated to $\tau = 1.75$ and $a = 1.42 \times 10^6\,m^{-1}$, respectively. However, these numbers were derived with the assumption, that the CCL layer exhibits a microstructure similar to a sintered electrode structure. As this is not the case here, the derived values for the specific surface area and the tortuosity can only serve as an estimate. For these numbers the model then predicts an area specific resistance of $ASR_{chem,calc} = 1.44\,\Omega\,cm^2$ at 600 °C.

Experimentally, a twice as high value was determined with $ASR_{chem,meas} = 2.85\,\Omega\,cm^2$ at 600 °C. For this, a cathode made of the LSC current collector layer only was electrochemically characterized in a symmetric setup. The current collector was applied by screen printing as a 30 μm thick layer and was characterized in an unsintered state on a GCO pellet in stagnant air. The comparably high polarization losses measured for this type of cathode can be attributed to the poor interface between the cathode and the electrolyte and to the fact, that the cathode particles are not sintered to each other.

As the measured value is more than 100 times higher and the calculated value is still more than 60 times higher than the lowest value measured on a nanoscaled thin film cathode ($ASR_{chem,min}$) and since they are still 17 and 9 times higher than the highest ($ASR_{chem,max}$), respectively, the influence of the current collector on the electrochemical performance can be considered negligible for such high performance cathodes (see Table 3).

3.4. Performance evaluation

Fig. 7 depicts a comparison of the results form this study to the results reported by Peters et al. [8], who investigated MOD derived nanoscaled $La_{0.5}Sr_{0.5}CoO_{3-\delta}$ thin film cathodes processed at $T_{max} = 900\,°C$. Polarization losses as low as $ASR_{chem} = 0.023\,\Omega\,cm^2$ at 600 °C were measured, easily satisfying the target value of

**Table 3**
Area specific polarization resistance values of a μm scaled LSC current collector layer determined by 1D model calculations ($ASR_{chem,calc}$) and EIS measurement ($ASR_{chem,meas}$) in comparison to the highest and lowest area specific resistance values measured on nanoscaled cathodes ($ASR_{chem,max}$ and $ASR_{chem,min}$).

μm scaled LSC CCL		nanoscaled thin film cathodes	
$ASR_{chem,calc}$ ($\Omega\,cm^2$)	$ASR_{chem,meas}$ ($\Omega\,cm^2$)	$ASR_{chem,min}$ ($\Omega\,cm^2$)	$ASR_{chem,max}$ ($\Omega\,cm^2$)
1.44	2.85	0.023	0.165
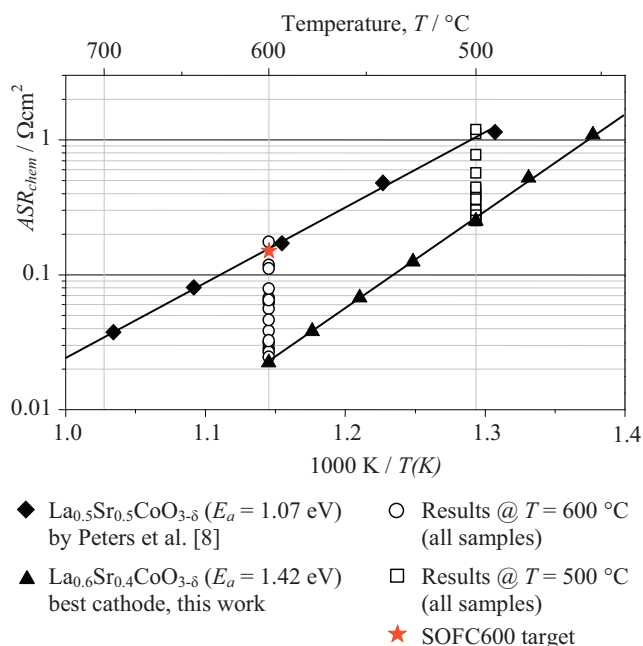
Fig. 7. Arrhenius plot of the results by Peters et al. [8] (◆) and the best nanoscaled La$_{0.6}$Sr$_{0.4}$CoO$_{3-\delta}$ thin film cathode (T_{max} = 700 °C, t_{an} = 0 h and ΔT = 3 K min^{-1}) measured in this study (▲). The open symbols represent results from all prepared samples measured at 500 °C (□) and 600 °C (○). The target value of the SOFC600 project is given as a benchmark.
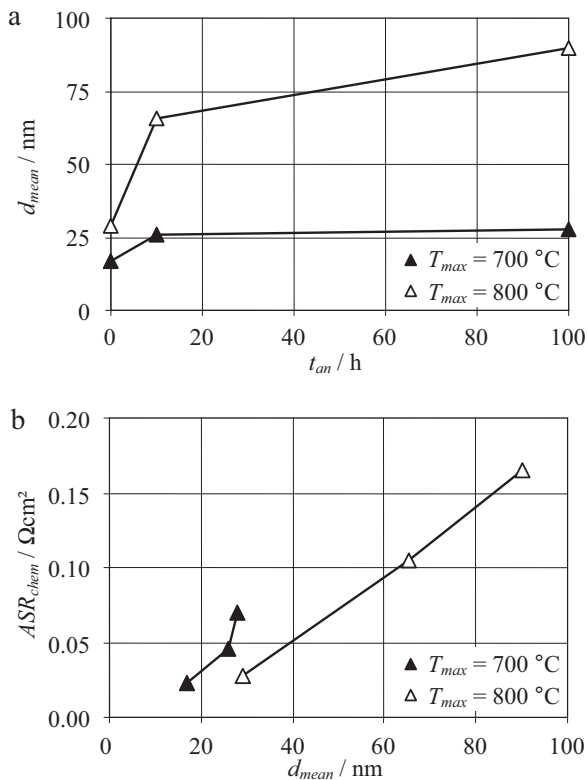
Fig. 8. The two graphs depict (a) the microstructure analysis results and (b) the performance analysis results of the samples prepared with the slow heating rate (ΔT = 3 K min^{-1}) in more detail. Graph (a) summarizes the determined mean grains size (d_{mean}) with respect to the annealing time. Graph (b) plots the measured area specific polarization losses at 600 °C over the mean grain size.

0.15 Ω cm^2 of the European project SOFC600 (FP6-2004-Energy-3, contract no. 020089). This value was determined for the cathode with the highest porosity of ε = 45% and the smallest average grain size of d_{mean} = 17 nm (see Figs. 3(a) and 4(a)), which therefore exhibited the largest surface area for the oxygen surface exchange reaction. The results of the other samples processed according to Table 1 fall in between the two graphs with polarization losses in the range of 0.023–0.165 Ω cm^2 at 600 °C. All cathodes exhibited nearly the same activation energy of E_a = 1.41 ± 0.03 eV. As the cathodic reaction was determined to be surface controlled for these thin film cathodes [6], this value is in good agreement with the activation energy of E_a = 1.3 ± 0.1 eV Baumann et al. [24] reported for the resistance associated with the oxygen surface exchange of La$_{0.6}$Sr$_{0.4}$CoO$_{3-\delta}$. Peters et al. [8] determined their La$_{0.5}$Sr$_{0.5}$CoO$_{3-\delta}$ thin film cathodes to be surface exchange controlled as well, with an activation energy of E_a = 1.07 eV. In good agreement with the trend, that the activation energy of the oxygen surface exchange coefficient decreases with increasing Sr-content [25], a lower activation energy was observed.

The results of the samples prepared with the slow heating rate (3 K min^{-1}) are displayed in more detail in Fig. 8. As depicted in Fig. 8(a), for a maximum processing temperature of 700 °C most of the grain growth occurred within the first 10 hours. After another 90 h, no significant change was observed. However, as the porosity decreased with increasing annealing time, the surface area available for the electrochemical reaction was reduced, leading to an increase of the area specific polarization losses. According to Adler et al. [19] the ASR_{chem} is inversely proportional to the volume specific surface area, if the cathode is surface exchange controlled. This effect is even more obvious if the samples prepared at 700 °C with 10 h (Fig. 3(b)) and 100 h (Fig. 3(c)) of annealing are compared to the sample prepared at 800 °C with 0 h of annealing (Fig. 3(d)). The grain sizes are about the same, however the ASR_{chem} is significantly lower for the latter sample. This is attributed to the comparably large open porosity. Sample annealing at 800 °C for 10 h (Fig. 3(e)) and 100 h (Fig. 3(f)) lead to a continuing grain growth and dense films, reducing the sites for the cathodic reaction to the comparably small surface area of the cathode film surface. The resulting losses are therefore comparably high.

Theoretical considerations on the reason for the high performance which these layers exhibit, including the comparison of the measured data to the results of the 1D model by Adler et al. [7,19] and a 3D finite element method model by Rüger et al. [22], not only ascribed the high performance to the increased inner surface area available for the electrochemical reaction, resulting from the nanoscaled microstructure, but also to increased oxygen surface exchange properties found for nanoscaled LSC thin film cathodes derived by MOD [6].[1] This enhanced oxygen surface exchange may be linked to the occurrence of small cobalt rich precipitations in the surface layer of the thin films, as preliminary results of the chemical analysis performed by TEM revealed. Such surface near cobalt rich phases were also observed by Wang et al. [21] on pulsed laser deposition (PLD) derived nanoscaled La$_{0.5}$Sr$_{0.5}$CoO$_{3-\delta}$ cathodes, however no enhanced surface exchange was observed. A more detailed and extensive analysis covering this topic is currently in progress.

In Fig. 9 polarization losses of different MIEC cathodes exhibiting a nanoscaled microstructure are plotted. It is by far not a complete literature overview, however good representatives from promising material systems ((Ba,La,Sr)(Co,Fe)O$_{3-\delta}$, (La,Sr)(Co,Fe)O$_{3-\delta}$ and (La,Sr)CoO$_{3-\delta}$) and configurations (with or without an additional

---

[1] In Ref. [6] all ASR_{chem} values calculated with the 1D model by Adler et al. are by a factor of 2 too high, resulting from a mistake in the corresponding equation (factor of 2). However, this does not affect the conclusions.
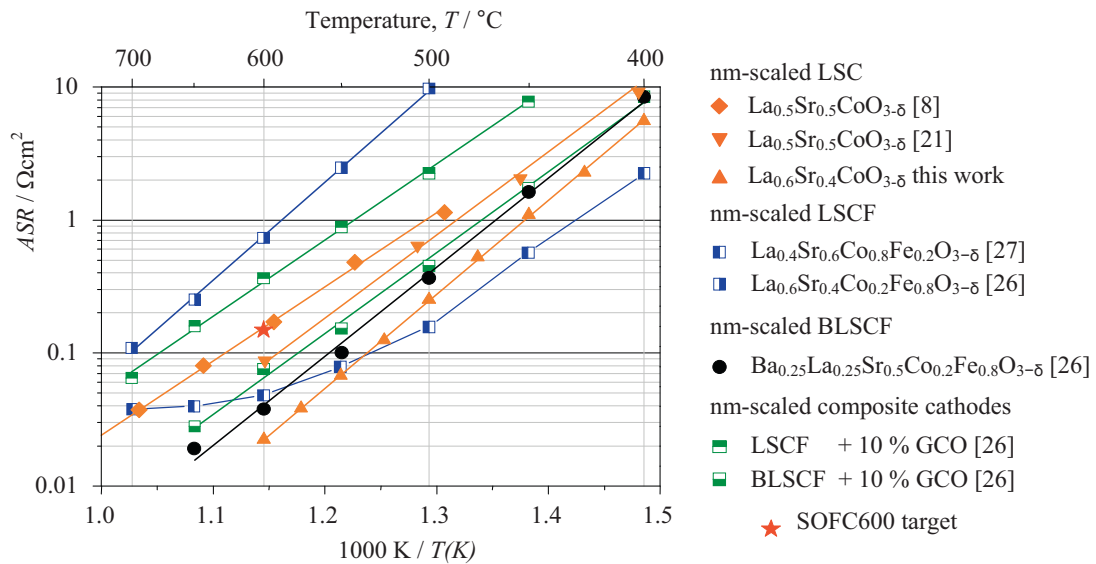
Fig. 9. Performance comparison of the best nanoscaled LSC thin film cathode presented in this work with other nanoscaled MIEC cathodes reported about in literature.

Table 4
Additional information on the cathodes presented in Fig. 9.

Cathode	Electrolyte	l_{Cat} (µm)	T_{max} (°C)	Time @ T_{max} (h)	d_{mean} (nm)	ASR @ 600 °C (Ω cm²)	E_a (eV)	Reference
$La_{0.6}Sr_{0.4}CoO_{3-\delta}$ [a]	GCO	0.2	700	0	17	0.023	1.42	This work
$La_{0.6}Sr_{0.4}Co_{0.8}Fe_{0.2}O_{3-\delta}$ [b]	GCO	10	800	6	130 ± 30	0.048	–	[27]
$La_{0.5}Sr_{0.5}CoO_{3-\delta}$ [a]	GCO on 8YSZ	0.3	900	0.1	54 ± 25	0.15	1.07	[8]
$La_{0.6}Sr_{0.4}Co_{0.2}Fe_{0.8}O_{3-\delta}$ [b]	GCO on 8YSZ	<1	750	10	<68	0.25	1.47	[26]
$La_{0.6}Sr_{0.4}Co_{0.2}Fe_{0.8}O_{3-\delta} + Ce_{0.8}Gd_{0.2}O_{1.9}$ [b]	GCO on 8YSZ	<1	750	10	<68	0.16	1.13	[26]
$Ba_{0.25}La_{0.25}Sr_{0.5}Co_{0.2}Fe_{0.8}O_{3-\delta}$ [b]	GCO on 8YSZ	<1	700	10	<68	0.038	1.33	[26]
$Ba_{0.25}La_{0.25}Sr_{0.5}Co_{0.2}Fe_{0.8}O_{3-\delta} + Ce_{0.8}Gd_{0.2}O_{1.9}$ [b]	GCO on 8YSZ	<1	700	10	<68	0.076	1.20	[26]
$La_{0.5}Sr_{0.5}CoO_{3-\delta}$ [c]	GCO	0.72	500	–	8 (50[d])	0.089	1.24	[21]

[a] Applied by metal organic deposition, followed by a high temperature step.
[b] Applied by spin coating, followed by a sintering step.
[c] Applied by pulsed laser deposition at elevated temperatures.
[d] Average grain size in the columnar basic structure.

electrolyte phase in the cathode structure) for intermediate temperature application were chosen for comparison with the data presented in this work [8,21,26,27]. Detailed information on the different configurations can be found in Table 4. Besides the cathodes by Baqué et al. [27] at low temperatures, MOD derived LSC thin film cathodes exhibit an excellent performance and impressively point out the potential of nanoscaled cathode technology for operating temperatures of 600 °C and lower.

4. Conclusions

Nanoscaled, phase pure $La_{0.6}Sr_{0.4}CoO_{3-\delta}$ thin film cathodes were prepared by metal organic deposition. By varying the processing parameters maximum processing temperature, heating rate and annealing time, the microstructure could be controlled in terms of grain size (17–90 nm) and porosity (0–45%). The sample with the smallest grain size and the highest porosity exhibited an area specific polarization resistance as low as $ASR_{chem} = 0.023\ \Omega\ cm^2$ at 600 °C. This was facilitated by a substantial increase of the inner surface area available for the oxygen surface exchange reaction, resulting from the nanoscaled microstructure and enhanced oxygen surface exchange properties of LSC derived by MOD. However, these results also lead to the conclusion, that nanoscaled LSC is limited to operation temperatures of ≤600 °C, since the microstructure coarsens at temperatures of 700 °C and higher. A general conclusion concerning degradation cannot be given at this point, as degradation and poisoning effects have to be analyzed in detail [28,29].

However, a first long term test (300 h) at 600 °C revealed, that after an initial degradation within the first 50 h, the best performing cathode stabilized at an $ASR_{chem} = 0.035\ \Omega\ cm^2$ at 600 °C.

Furthermore, it was demonstrated experimentally and analytically, that a current collector with µm sized particles can be applied to contact high performance nanoscaled cathodes, without having a (positive) influence on the cathode's electrochemistry.

To our knowledge, the area specific polarization resistances reported in this work are the lowest reported in literature for 600 °C. Future work will concentrate on detailed electrochemical modeling of nanoscaled LSC thin film cathodes, detailed microstructural and chemical analysis and stability investigations.

References

[1] H. Timmermann, W. Sawady, R. Reimert, E. Ivers-Tiffée, J. Power Sources 195 (2010) 214–222.
[2] D. Nikbin, Fuel Cell Rev. 3 (2006) 21–24.
[3] O. Yamamoto, in: W. Vielstich, A. Lamm, H.A. Gasteiger (Eds.), Handbook of Fuel Cells, vol. 4, John Wiley & Sons Ltd., Chichester, England, 2003, pp. 1002–1014.
[4] E. Ivers-Tiffée, U. Guntow, J. Hayd, B. Rüger, Proceedings of the 8th European Solid Oxide Fuel Cell Forum, 2008, p. A0403.
[5] B. Rüger, Mikrostrukturmodellierung von Elektroden für die Festelektrolyt-brennstoffzelle, Universitätsverlag Karlsruhe, Karlsruhe, 2009.
[6] J. Hayd, U. Guntow, E. Ivers-Tiffée, ECS Trans. 28 (2010) 3–15.
[7] S.B. Adler, J.A. Lane, B.C.H. Steele, J. Electrochem. Soc. 143 (1996) 3554–3564.
[8] C. Peters, A. Weber, E. Ivers-Tiffée, J. Electrochem. Soc. 155 (2008) B730–B737.
[9] K. Huang, M. Feng, J.B. Goodenough, C. Milliken, J. Electrochem. Soc. 144 (1997) 3620–3624.
[10] A. Mai, V.A.C. Haanappel, S. Uhlenbruck, F. Tietz, D. Stöver, Solid State Ionics 176 (2005) 1341–1350.
[11] E. Bucher, A. Egger, G.B. Caraman, W. Sitte, J. Electrochem. Soc. 155 (2008) B1218–B1224.
[12] L. Dieterle, B. Butz, D. Fuchs, MC2009 2 (2009) 395–396.
[13] P. Gilbert, J. Theor. Biol. 36 (1972) 105–117.
[14] A. Weber, A.C. Müller, D. Herbstritt, E. Ivers-Tiffée, Proceedings of the Seventh International Symposium on Solid Oxide Fuel Cells (SOFC-VII), 2001, pp. 952–962.
[15] H. Schichlein, A.C. Müller, M. Voigts, A. Krügel, E. Ivers-Tiffée, J. Appl. Electrochem. 32 (2002) 875–882.
[16] R.H.E. van Doorn, Dissertation, University of Twente, 1996.
[17] G. Brauer, H. Gradinger, Z. Anorg. Allg. Chem. 276 (1954) 209–226.
[18] S.B. Adler, Chem. Rev. 104 (2004) 4791–4843.
[19] S.B. Adler, Solid State Ionics 111 (1998) 125–134.
[20] A. Leonide, V. Sonn, A. Weber, E. Ivers-Tiffée, ECS Trans. 7 (2007) 521–531.
[21] S. Wang, J. Yoon, G. Kim, D. Huang, H. Wang, A.J. Jacobson, Chem. Mater. 22 (2010) 776–782.
[22] B. Rüger, A. Weber, E. Ivers-Tiffée, ECS Trans. 7 (2007) 2065–2074.
[23] J. Joos, T. Carraro, B. Rüger, A. Weber, E. Ivers-Tiffée, ECS Trans. 28 (2010) 81–91.
[24] F.S. Baumann, J. Fleig, G. Cristiani, B. Stuhlhofer, H.U. Habermeier, J. Maier, J. Electrochem. Soc. 154 (2007) B931–B941.
[25] A.V. Berenov, A. Atkinson, J.A. Kilner, E. Bucher, W. Sitte, Solid State Ionics 181 (2010) 819–826.
[26] A.J. Darbandi, H. Hahn, Solid State Ionics 180 (2009) 1379–1387.
[27] L. Baqué, E. Djurado, C. Rossignol, D. Marinha, A. Caneiro, A. Serquis, ECS Trans. 25 (2009) 2473–2480.
[28] P. Hjalmarsson, M. Sogaard, M. Mogensen, Solid State Ionics 179 (2008) 1422–1426.
[29] H. Yokokawa, in: W. Vielstich, H. Yokokawa, H.A. Gasteiger (Eds.), Handbook of Fuel Cells—Fundamentals, Technology and Applications, John Wiley & Sons Ltd., Chichester, 2009, pp. 924–932.